Peer reviewed version

University of Bristol - Explore Bristol Research
General rights

Structure of levitated Si-Ge melts studied by high-energy x-ray diffraction in combination with reverse Monte Carlo simulations

Irina Pozdnyakova[1], Oleksandr Roik[2], James W. E. Drewitt[3] Aleksei Bytchkov[4], Florian Kargl[5], Sandro Jahn[6], Séverine Brassamin[1], Louis Hennet[1,7]

[1] Conditions Extrêmes et Matériaux : Haute Température et Irradiation, CNRS, Université d'Orléans, 45071 Orléans cedex 2, France
[2] National Taras Shevchenko University of Kyiv, 01033 Kyiv, Ukraine
[3] School of Physics, University of Bristol, HH Wills Physics Laboratory, Tyndall Avenue, Bristol, BS8 1TL
[4] ESRF-The European Synchrotron, 38043 Grenoble Cedex 9, France, France
[5] Institut für Materialphysik im Weltraum, Deutsches Zentrum für Luft- und Raumfahrt (DLR), 51170 Köln, Germany
[6] Institute of Geology and Mineralogy, University of Cologne, Zülpicher Str. 49b, 50674 Köln, Germany
[7] Interfaces, Confinement, Matériaux et Nanostructures, CNRS, Université d'Orléans, 45071 Orléans cedex 2, France

E-mail: louis.hennet@cnrs-orleans.fr

Abstract

The short-range order in liquid Si, Ge and binary Si_x-Ge_{1-x} alloys ($x = 0.25, 0.50, 0.75$) was studied by x-ray diffraction and reverse Monte Carlo simulations. Experiments were performed in the normal and supercooled liquid states by using the containerless technique of aerodynamic levitation with CO_2 laser heating, enabling deeper supercooling of liquid Si and Si-Ge alloys than that previously reported. The local atomic structure of liquid Si and Ge is found to resemble the β-tin structure. The first coordination numbers of about 6 for all compositions are found to be independent of temperature indicating the supercooled liquids studied retain this high-density liquid (HDL) structure. However, there is evidence of developing local tetrahedral ordering, as manifested by a shoulder on the right side of the first peak in $S(Q)$ which becomes more prominent with increasing supercooling. This result is potentially indicative of a continuous transition from the stable HDL β-tin (high pressure) phase, towards a metastable low-density liquid (LDL) phase, reminiscent of the diamond (ambient pressure) structure.

Keywords: Aerodynamic levitation, SiGe melts, liquid structure, Synchrotron x-ray diffraction, RMC

1. Introduction

Silicon and germanium are the only group IV elements that are fully miscible, forming a continuous series of substitutional solid alloys. In the crystalline form at room pressure, these substances have a diamond lattice structure - an open structure with a coordination number of four. The lattice constants of the alloys depend linearly on their concentration, following Vegard's law, and their properties change continuously with concentration [1]. There is significant practical importance for these alloys and their end-members for semiconductor applications. Monocrystalline silicon is the most widely used host material in the integrated electronics industry. Si-Ge heterojunction bipolar transistor technology was first developed at IBM [2]. It is now widely used in various communication applications and still studied for next generation technologies [3]. Applications range from wired and wireless communications circuits to disk storages

and high-speed high-bandwidth instrumentation [4]. Single crystal Si-Ge materials are typically grown from the melt via the Czochralski process [5]. Information on the liquid structure of Si-Ge compounds is therefore important for understanding and optimising the fabrication of these highly demanded industrial materials.

Silicon and germanium both undergo a semiconductor to liquid metal transition upon melting from the crystalline solid, which is accompanied by an anomalous ~ 10 % (Si) and 6 % (Ge) volume contraction [6,7] and unusual negative slope in the high-pressure melting curves on initial compression [8]. Diffraction experiments reveal average coordination numbers of around 6-7 in the liquid-state [9-15], significantly lower than the value of ~11-12 observed in most liquid metals with simple close packed [16] or bcc [17] structures in the solid state. Similar anomalous melting curves with negative pressure dependence accompanied by densification on melting is classically observed in H_2O ice-water transition (ice floats on water) and reported in some other complex low coordinated elemental liquids (e.g. Ga, Bi, Sb) and is typically accompanied by a crystalline phase transition with large volume change below the solidus temperature. If remnants of both (high- and low-density) crystalline phases are transferred into the liquid state then this anomalous melting behaviour may be explained by the continuous transition between these low-density liquid (LDL) and high-density liquid (HDL) local structures with pressure [18], implying the existence of a melting curve maximum at negative (tensile-strained) pressure similar to melting curve maxima observed in other anomalous liquid systems [19]. Detailed experimental structural studies of high temperature and supercooled liquid Si, Ge, and their alloys are, therefore, important for understanding the melting behaviour of these complex liquids and relationship to solid-state structure and properties.

The structure of pure levitated liquid Si has been measured by x-ray diffraction to temperatures extending 143 K into the supercooled liquid regime below the melting point T_m [13]. The local structure of pure liquid Ge has also been studied 300 K into the supercooled regime by x-ray absorption spectroscopy (XAS) using a graphite oven [20]. Molecular dynamics (MD) simulations combined with ambient temperature high-pressure data indicate the existence of an LDL-HDL transition in deeply supercooled Si and Ge liquids [21]. At normal pressure, this LDL-HDL transition is expected to occur at about 1060K [22], approximately 300K below the lowest supercooling previously reported (for liquid Si [23]) and is thus difficult to access experimentally.

Only a few experimental studies of the melt structure of Si_x-Ge_{1-x} alloys have been reported. Inui et al. measured the x-ray absorption spectra of various melt compositions from $x = 0$ to 0.6 at the Ge absorption edge [24], suggesting a slight decrease in the nearest neighbour distances r_{Ge-Ge} and r_{Ge-Si} with increasing temperature, and an increase in both distances

with higher silica fractions. Naito et al. reported the structure of melt compositions $x = 0$, 0.3, 0.5, 1 using energy-dispersive x-ray diffraction and found the first peak position in $g(r)$ remains relatively stable with increasing temperature, moving to shorter distances with increasing Si content [14]. These authors report average coordination numbers of ~ 5-6, with most values in agreement within experimental uncertainty regardless of composition or temperature when using a consistent integration method. Both studies were performed using a conventional furnace with all measurements made above the melting point. Using the containerless method of aerodynamic levitation, Krishan et al. measured the structure of $Si_{0.5}Ge_{0.5}$ melts in the supercooled region at temperatures 120 K below T_m [15]. The position of the first peak in $g(r)$ and coordination number of ~6 were found to be invariant with temperature. An *ab initio* molecular dynamics (MD) study of the electronic structure and properties of liquid $Si_{0.5}Ge_{0.5}$ showed the alloy has a predominantly random structural arrangement of Si and Ge with a slight preference for Si–Si and Ge–Ge bonds, and exhibits metallic conductivity characteristics [25]. A recent MD study of the thermophysical properties and atomic structure of Si-Ge melts predicts some development in structural ordering during cooling from the stable liquid into the supercooled regime [26].

In this work, we report the structural properties of liquid $Si_{0.5}Ge_{0.5}$, $Si_{0.75}Ge_{0.25}$ and $Si_{0.25}Ge_{0.75}$ alloys in the stable and supercooled liquid states using *in situ* synchrotron x-ray diffraction with aerodynamic levitation. We also measured the structure of liquid Si with deeper supercooling (385 K below T_m) than previously reported, and report measurements of liquid Ge at ~ 90 K below T_m. The atomic structure of the stable and supercooled liquid states was refined using reverse Monte Carlo (RMC) simulations constrained to the diffraction measurements.

2. Experimental methods

All samples were prepared from silicon and germanium powders (purity 99.999% from Alfa Aesar) in a 2-step process. First, compacted pellets formed from mixed powders of the required stoichiometry for the alloys were formed using a powder press in an argon-filled glove box (less than 3ppm O_2). Spherical samples (2.7 mm in diameter) were then formed by melting these pellets using aerodynamic levitation and CO_2 laser heating [27]. To avoid oxidation, the levitation chamber was first evacuated to 10^{-5} mbar and then refilled with the same pure argon (Air Liquide, < 0.1ppm O_2) gas used for levitating the sample.

The x-ray diffraction experiments were performed at the ID11 beam line at European Synchrotron Radiation Facility (ESRF) in Grenoble, France, with an incident x-ray beam energy of 79.72 keV. The scattered intensity was measured in transmission geometry using a 10 x 10 cm^2 "Frelon" high-resolution fast CCD detector, developed at the ESRF [28]. A

cylindrical lead beam stop with a diameter of 3 mm was used to protect the detector from the direct beam. The acquisition time for each liquid diffraction measurement was 60 s. The distance between the sample and the image plate was 194 mm, giving a reasonable usable Q-range of 0.8-16 Å^{-1}. One-dimensional diffraction patterns were obtained by integrating the two-dimensional diffraction patterns using the FIT2D software package [29]. The detector calibration was performed using Ni and Si spheres.
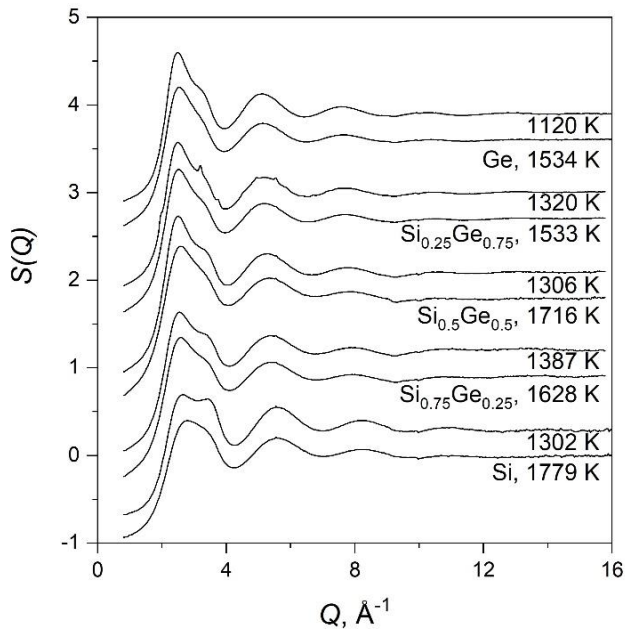

Figure 1. Total x-ray structure factor $S(Q)$ for liquid Si-Ge alloys at different temperatures. The data are shifted vertically for clarity.

The samples were melted using the containerless method of aerodynamic levitation with CO_2 laser heating. This technique offers a high degree of supercooling [15] and is well suited for, and readily integrated into, a wide range of different experimental setups at synchrotron and neutron beamlines [30]. A detailed description of the levitation setup is given elsewhere [31]. The spherical sample is placed in a convergent-divergent nozzle that directs a gas jet supporting the sample. Then the sample is melted using two 125 W CO_2 laser beams focused onto the sample by means of spherical mirrors. As for the sample fabrication step, the levitation chamber was pre-evacuated to 10^{-5} mbar before refilling with the pure argon (Air Products, < 0.01ppm O_2) levitation gas prior to each measurement.

Temperature was measured using a single-color infrared pyrometer, operating at $\lambda = 1.625$ µm, focused at the top of the sample. The calibration procedure described in Ref. [32] was applied. To check this calibration, we recorded temperatures during the free cooling of the sample after turning off the laser. The recalescence temperature was then checked for agreement with the expected liquidus temperature from the phase diagram [33]. In order to minimize the temperature gradient, the top laser is incident on the sample at

an angle of 20° from the vertical axis around which the sample rotate rapidly during levitation. The temperature gradient is further reduced by the second laser incident on the bottom of the sample to compensate for the cooling from the gas flow. Temperature homogenisation within the sample is also enhanced by the good thermal conductivities of the alloy components, close to that of metallic melts. (~57 W/mK at 1700 K for Si and 43 W/mK at 1273 K for Ge [34]). The residual temperature gradient is estimated to be less than 10K in all measurements.

The total structure factors $S(Q)$ were extracted from the experimental data using the procedure described in detail in Drewitt et al. [35]. The data were corrected for background, absorption by the sample, and self and Compton scattering contributions. The pair correlation function $g(r)$ is calculated from $S(Q)$ via the Fourier transform relation:

$$g(r) = 1 + \frac{1}{2\pi^2 \rho_0} \int_0^{Q_{max}} Q(S(Q)-1)\frac{\sin Qr}{r}M(Q)dQ, \quad (1)$$

where ρ_0 is the number of atoms per unit volume. $M(Q)$ is a modification function used to reduce the termination ripples in the Fourier transform arising from the finite maximum scattering vector Q_{max} in the experimental measurements. In this study, we used the Lorch modification function. The temperature dependent number density was calculated from the molar volumes of the pure elements [36,37] assuming ideal mixing. Although the average coordination numbers C_1 can be determined by different methods, we adopted the method used by Naito et al. [14] by taking twice the value obtained by integrating the first peak of the radial distribution function $RDF(r) = 4\pi\rho_0 r^2 g(r)$ up to the maximum of the first peak at distance r_1.
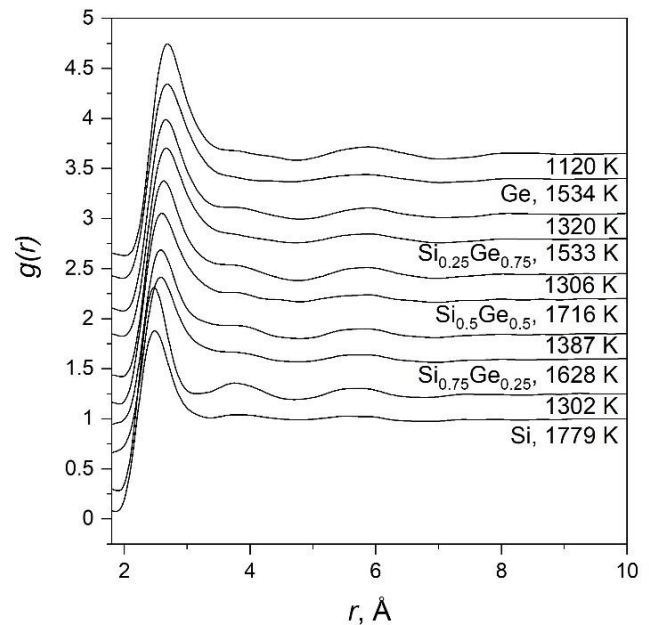

Figure 2. Total pair correlation function $g(r)$ for liquid Si-Ge alloys at different temperatures. The data are shifted vertically for clarity

The structural parameters obtained for the compositions studied are summarized in Table 1 together with the melting points taken from the Si-Ge phase diagram [33]. The temperatures of the supercooled liquids are shown in bold italic giving a maximum supercooling of 385 K for Si, 238, 244 and 120 K for the alloys and 91 K for Ge. The absolute uncertainties in the peak positions and coordination numbers are estimated at $\pm$ 0.02 Å and $\pm$ 0.5, respectively. The peak positions in the $S(Q)$ and $g(r)$ functions are in excellent agreement with previous studies [9-15].
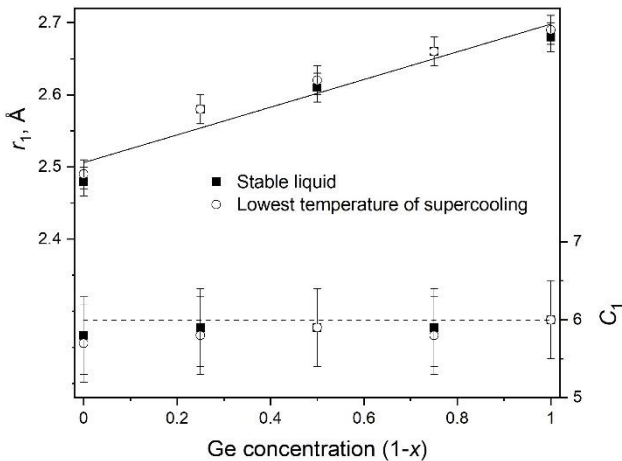

Figure 3. Ge-concentration dependencies of the first interatomic distances r_1 (top) and coordination numbers C_1 (bottom) in the stable liquid and at the lowest temperature of supercooling. The values C_1 and r_1 remain constant over the studied temperature range within the experimental uncertainty. The solid straight line represents a linear fit to the stable liquid data. The dashed line corresponds to $C_1=6$.

3. Simulation details

Reverse Monte Carlo (RMC) simulations [38] were performed using the RMCA version 3.14 package to generate structural models of the Si and Ge liquids and their binary Si_xGe_{1-x} alloys. The final atomistic configurations were generated by iteratively minimising the difference between the $S(Q)$ measurements and the structural model. A starting cubic cell with periodic boundary conditions contained 10^4 randomly arranged atoms. The volume of the cubic cells was adjusted to match the atomic number density (ρ_0) of each alloy measured by x-ray diffraction at the temperatures reported in table 1. Distances of the closest approach for two atoms d(Si-Si) = 1.95 Å and d(Ge–Ge) = 2.15 Å were estimated from the experimental pair correlation functions of the pure liquids. The distance of closest approach cut-off distance between Si and Ge atoms was taken as 2.05 Å (computed as arithmetic average of d(Si-Si) and d(Ge–Ge). The initial value of random atomic movement was 0.5 Å, reducing to 0.05 Å during simulation.

The RMC-models were analysed using Voronoi tessellation, a common descriptor of the local structure in a disordered system [39]. In Voronoi tessellation (also called a

Voronoi diagram) the model volume is divided into cells (Voronoi polyhedra) with an atom at the centre. Each Voronoi polyhedron (VP) encloses the region of space that is closer to the central atom than any other ones. Since the VP is the geometrical image of the local environment of the central atom, its metric and topological characteristics can be used to find the statistical regularities of the short-range order (SRO) in liquid alloys. One of the most informative metric characteristics of the VP is the sphericity coefficient ($K_{sph} = 36\pi V^2/S^3$, where V is the volume, and S is the surface area of the VP), that defines a deviation of the shape of the given VP from a regular sphere ($K_{sph} = 1$). The Voronoi diagram of the RMC-models was constructed using the algorithm described by Medvedev [40].

4. Results and discussion

The measured $S(Q)$ functions for the Si-Ge alloys and end member at the highest (stable liquids above T_m) and lowest (supercooled liquids) temperatures obtained for each sample are shown in Figure 1. All the $S(Q)$ functions share similar characteristics, with three distinct peaks and a shoulder on the high-Q side of the first peak, which becomes increasingly prominent with deeper supercooling. The position of the first peak varies from ~ 2.5 Å^{-1} for liquid Ge to ~ 2.7 Å^{-1} for liquid Si. The shoulder appears in the region from 3.2 to 3.4 Å^{-1}. There is a slight shift in the first peak to lower Q with deeper supercooling for all alloys, as previously observed for liquid Si [15]. The $S(Q)$ for the $Si_{0.25}Ge_{0.75}$ alloy at 1320 K contains minor Bragg peak contamination due to onset crystallization of the melt towards the end of the measurements. However, as crystalline Bragg scattering is much more intense compared to liquid diffuse scattering, it is obvious that this crystalline contamination is negligible compared to the bulk liquid contribution and should not affect the structural parameters. The corresponding real-space $g(r)$ functions are shown in Figure 2. For all compositions, the bond distance r_1 and nearest-neighbour coordination numbers C_1 remain independent of temperature (within the absolute errors) across the experimentally accessible temperature range, even at considerable supercooling, consistent with previous studies [14,15,23]. Distinct changes are, however, apparent in the second and higher coordination spheres.

The first peak position at $r_1 = 2.48$ Å for pure Si gradually shifts to higher distances with increasing Ge concentration in the alloy to 2.57 Å ($x = 0.75$), 2.62 Å ($x = 0.5$), 2.66 Å ($x = 0.25$) and 2.68 Å for pure Ge. This trend is plotted in Figure 3, together with the corresponding C_1 values, at the highest and lowest measured temperatures. The distance r_1 for the alloys deviates slightly from a linear evolution if constrained to the absolute values for the end members, which may indicate a slight tendency towards more homoatomic bonding as predicted by Ko et al. [25]. However, the weighted fit to the stable liquid data (as shown in Fig. 3) reveals a quasi-

linear evolution of r_1 over the studied composition range within the experimental uncertainty. Additional investigations are required to provide firm conclusions on the preferential bonding nature in these alloys. In agreement with previous x-ray diffraction studies [13,23], the average coordination number C_1 remains ~ 6 for all compositions (within the absolute errors), although, as noted in an earlier study [10], C_1 is ill-defined in the pure liquid Ge measurements ranging from ~ 5.7 to ~ 7.5 depending on the limit of integration used. If there are any systematic changes in coordination number, these are small and below the resolution of the experiment.

It is useful to consider the classification of the structural properties of liquids according the scheme proposed by Price and Moss [41]. In this scheme, the main peaks in $S(Q)$ are used to identify the type of ordering that may exist in the liquid or glass by scaling Q_1 with r_1 (both tabulated in table 1), the first-nearest-neighbour distance, and d_s, the mean interatomic spacing ($\rho_0^{-1} = (\pi/6)d_s^3$). Figure 4 shows Q_1r_1 plotted against Q_1d_s for all the liquids studied here. It is clear that all the liquid compositions studied depart significantly from the dense random packing limit of hard spheres, indicated by the solid line in figure 4. The Q_1r_1 values between (6.5 and 6.8) are higher than the characteristic values expected for tetrahedral network forming liquids (~4.5) and approach those for metallic glasses (~7.5) [42].
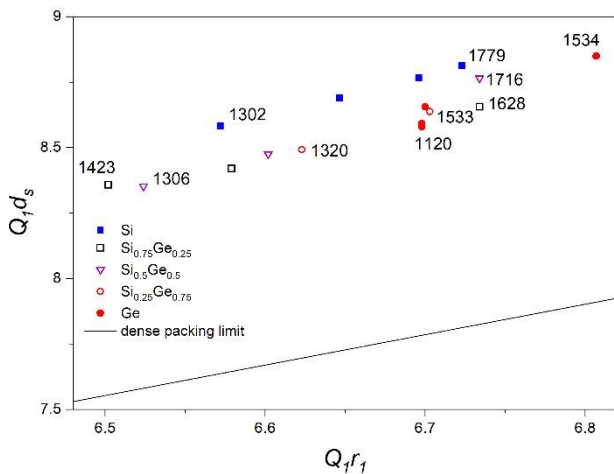

Figure 4. Scattering vectors of the first peaks in the structure factors $S(Q)$ of liquid alloys, scaled by the nearest-neighbour distance r_1 and the mean interatomic spacing d_s. The corresponding dense packing limit is shown for reference. The values next to the data points indicate the temperature in Kelvin.

The RMC simulations can provide some more detailed insight into the local structure organization. The RMC derived structure factors for liquid Si, Ge, and their binary Si_xGe_{1-x} alloys are shown in Figure 5 together with the experimental data at temperatures above (Fig. 5a) and below (Fig. 5b) the equilibrium liquidus line. The RMC simulations are in relatively good agreement with the experimental data. However, we note that RMC simulations have been shown by

Drewitt et al. [43] to converge to drastically different structures, depending on starting configurations, yet still exhibit almost identical $g(r)$ functions. Nevertheless, we note the RMC results do reproduce the observed shoulder in $S(Q)$ very well, and the local structure predicted from the RMC model is in good agreement with earlier experimental and theoretical findings. Further MD calculations using reliable empirical potentials or from first principles could also be employed to verify the RMC results presented here.
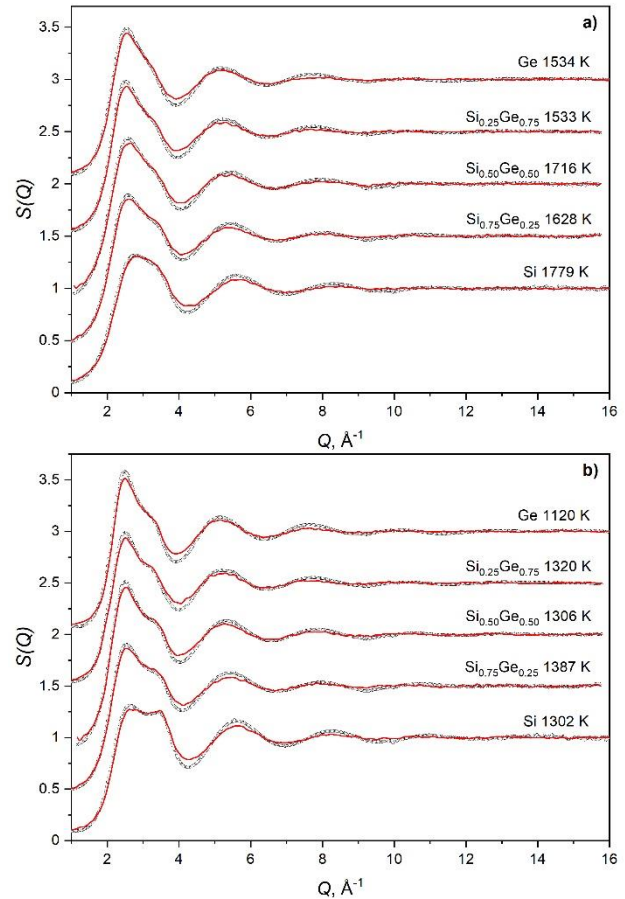

Figure 5. The $S(Q)$ functions for the stable (a) and supercooled (b) liquid Si, Ge, and Si_xGe_{1-x} alloys. The solid (red) lines denote the RMC results, whereas the open (black) circles show the experimental data.

The values of K_{sph} obtained from the VP analysis of liquid Si, Ge, and Si_xGe_{1-x} alloys vary from 0.63 for Si-centred polyhedra to 0.66 for Ge-centred motifs. For reference, K_{sph} of VPs for atoms in the ambient pressure (diamond) and high pressure (β-tin) crystal structures are 0.465 and 0.652, respectively, while $K_{sph}= 0.689$ for the dense non-crystalline packing typical of most liquid metals [44]. Therefore, liquid Si and Ge appear to have local atomic structures similar to β (white)-tin, in agreement with earlier experimental and theoretical findings [9,20,45-48]. In the β-tin structure, each atom has four nearest neighbours on a flattened tetrahedron and two other neighbours slightly further away on the

perpendicular to the plane of the flattened tetrahedron., giving a coordination number $C_1 = 4 + 2$, consistent with the values of $C_1 \sim 6$ obtained for all melts measured in this study.

The high-Q shoulder observed in the first peak in $S(Q)$ for liquid Si, Ge, and their binary alloys, is a key feature of category III liquid metals according to the Waseda classification [9], which includes other low coordinated elemental liquids including Ga ($C_1 \sim 10$ [49]), Sb ($C_1 \sim 8.5$ [50]), Bi ($C_1 \sim 8$ [51]), and Sn ($C_1 \sim 7.5$ [52]). This shoulder is associated with the Friedel oscillations induced by the conduction electrons, as shown for liquid Ga [53] and liquid group-IV elements [54], and its position is determined as $Q = 2k_F$, where k_F is the Fermi wavenumber of the conduction electrons. It was suggested that the covalent elements with anisotropic bonding in the solid state have a lower degree of symmetry in the liquid state than elements with isotropic metallic bonding, which is manifested by a shoulder in $S(Q)$, and this structure disappears at temperatures of 300-500K above the melting point [9]. Jank and Hafner performed molecular dynamics simulations of the atomic structure and self-consistent linear muffin-tin orbital supercell calculations of the electronic structure [54]. They showed that for the two light elements Si and Ge, the modulation of the random ionic packing by Friedel oscillations leads to a complex structure of the liquid with low coordination numbers, only short-range distance correlations, and weak covalent bonding effects. For the two heavier elements Sn and Pb, non-local relativistic effects lead to a damping of the Friedel oscillations and to a return to a hard sphere-like structure of the melt. [55]. Indeed, the shoulder in $S(Q)$ of liquid Sn is much less pronounced [9] in comparison to liquid Si and Ge.

Next, we attempt to rationalize the relationship between the shoulder in $S(Q)$ and the covalent bonding in the liquid using the refined RMC models for liquid Si and Ge. The latter have been analysed for the presence of short interatomic distances less than the length of the covalent bond in the crystal structures of Ge (0.245 nm) and Si (0.235 nm). The atomic configurations were divided into two parts: (1) atoms that have at least one neighbours at a distance less than and equal to the length of a covalent bond (type Cb – "Covalent bonding") and (2) all remaining atoms (type Mb – "Metal bonding"). Thus, pure liquid Si and Ge are considered as binary systems. The partial structure factors $S_{CbCb}(Q)$, $S_{CbMb}(Q)$, and $S_{MbMb}(Q)$ calculated from the RMC models using the Faber-Ziman formalism are shown in Figure 6. The position of the main peak in $S_{CbCb}(Q)$ coincides with the position of the shoulder observed in the first peak of the measured $S(Q)$. The first peaks in $S_{CbMb}(Q)$ and $S_{MbMb}(Q)$ on-the-other-hand coincide with the first peak of $S(Q)$. Since the individual contributions of the partials to the total structure factor depend on the atomic concentration of each component, the contribution of $S_{CbCb}(Q)$ curve is more significant in the $S(Q)$ of liquid Si leading to a more pronounced shoulder. It should be noted that the division

of the liquid structure into two subsystems ("covalent bonding" and "metal bonding") is somewhat arbitrary, because the only criterion for selection was the interatomic distance. However, our results already indicate that the cause of the shoulder appearance may be the presence of a subsystem that is characterized by shorter distances between the nearest atoms.
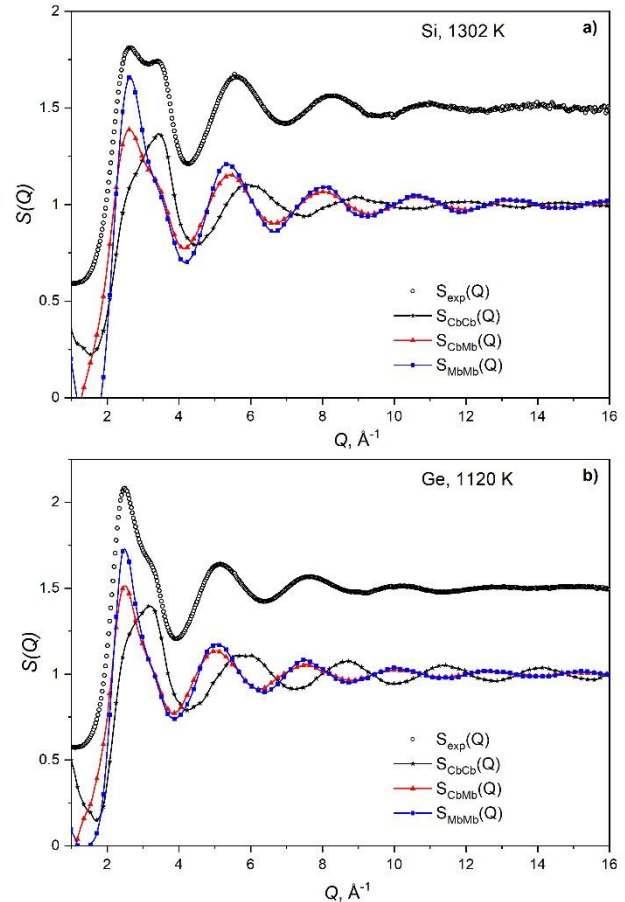

Figure 6. The experimental $S(Q)$ curves and the RMC partial $S_{CbCb}(Q)$, $S_{CbMb}(Q)$, and $S_{MbMb}(Q)$ curves for the liquid Si at 1302K (a) and Ge at 1120K (b). The experimental data are shifted up by 0.5 for clarity. The negative values in figure (b) are due to some shortcomings of the RMC simulations.

Various MD simulations on Si [21,22], Ge [56] and SiGe [25], attribute the high-Q shoulder on the first peak in $S(Q)$ to a signature of a tetrahedral structure which remains after melting and grows with decreasing temperature. Since liquid Si and Ge stabilize into the diamond structure upon solidification, it is reasonable to consider that the structural units with shorter bonds found in these liquids are tetrahedral.

However, it is difficult to unequivocally associate the evolution of this shoulder observed during supercooling to the development of this tetrahedral order, because we do not observe any reduction in the average coordination number, and all our liquids appear to have the same local order (see Fig.3). A recent neutron diffraction with isotopic substitution (NDIS) measurement of liquid $Si_{20}Ge_{80}$ attributes this

shoulder to a selective occupancy of Ge positions by Si in the $S_{SiGe}(Q)$ partial structure factor [57]

Nevertheless, MD simulations predict an increase in local tetrahedral order, and corresponding rapid decrease in average coordination number, with decreasing temperature during deep supercooling, at temperatures below ~ 750 K for Ge [58], and ~1100 K for Si [55]. These deeply supercooled states are beyond our experimental temperature range and difficult to access using aerodynamic levitation due to early crystallization at much lower temperatures. Interestingly, the relation between these "critical" temperatures and the corresponding melting temperatures is the same for liquid Ge and liquid Si: 750 K / 1211 K $\cong$ 1100 K / 1687 K.

Table 1. Summary of the structural parameters for all liquids studied in this work. Temperature: T, number density: ρ_0, position of the main peak and its shoulder in $S(Q)$: Q_1 and Q_{sh}, first peak position in $g(r)$: r_1 and coordination number C_1. Temperatures for the supercooled liquids are indicated in bold italic.

T (K) $\pm$ 20 K	ρ_0 (Å^{-3})	Q_1 (Å^{-1}) $\pm$ 0.05	Q_{sh} (Å^{-1}) $\pm$ 0.05	r_1 (Å) $\pm$ 0.02	C_1 $\pm$ 0.5
Si (T_m = 1687 K)					
1779	0.0550	2.7		2.48	5.8
1508	0.0559	2.7	3.33	2.48	5.6
1404	0.0561	2.68	3.35	2.48	5.6
1302	0.0563	2.65	3.43	2.49	5.7
Si$_{0.75}$Ge$_{0.25}$ (T_m ≈ 1625 K)					
1628	0.0524	2.61	3.36	2.58	5.9
1423	0.0530	2.53	3.38	2.57	5.8
1387	0.0531	2.55	3.4	2.58	5.8
Si$_{0.5}$Ge$_{0.5}$ (T_m ≈ 1550 K					
1716	0.0493	2.59	3.3	2.61	5.9
1432	0.0502	2.52	3.32	2.62	6.0
1306	0.0506	2.49	3.34	2.62	5.9
Si$_{0.25}$Ge$_{0.75}$ (T_m ≈ 1440 K)					
1533	0.0474	2.52	3.32	2.66	5.9
1320	0.0482	2.49	3.2	2.66	5.8
Ge (T_m = 1211 K)					
1534	0.0452	2.54	3.22	2.68	6.0
1303	0.0461	2.5	3.22	2.68	5.9
1181	0.0465	2.49	3.24	2.69	5.9
1120	0.0467	2.49	3.24	2.69	6.0

An increase in tetrahedral order with deeper supercooling could be indicative of a continuous transition from the stable HDL phase, reminiscent of β-tin (high pressure) structure, towards a metastable LDL phase, reminiscent of the diamond (ambient pressure) structure, accompanying the metal-semiconductor transition. Indeed, MD simulations combined with high-pressure data at ambient temperatures suggest the low-density liquid (LDL) – high-density liquid (HDL) phase transition in the deeply supercooled region for both Si and Ge [21]. More recently, ultrafast time-resolved x-ray emission spectroscopy measurements, using femtosecond free electron x-laser pulses, have observed the electronic structure of Si evolve from the solid, melting into a transient LDL phase prior

to the stable HDL phase transition in liquid Si [59]. If the liquid-liquid phase transition is continuous there will be some coexistence of metastable LDL clusters in the HDL matrix. Therefore, with deeper supercooling, the number of tetragonal LDL clusters grow causing Friedel oscillations to scatter more on these structural "defects" which is manifested as a development we observed in the shoulder of the first peak in $S(Q)$.

5. Conclusion

We have presented new high-energy x-ray diffraction measurements of the structure of Si, Ge, and Si$_x$-Ge$_{1-x}$ in the stable liquid and supercooled states at temperatures up to ~385 K (Si), ~90 K (Ge), and ~ 120-244 K (Si$_x$-Ge$_{1-x}$) below their melting temperatures. The nearest-neighbour interatomic distance increases linearly with increasing Ge concentration, although a slight deviation from linear behaviour due to the presence of homoatomic bonding cannot be excluded. All compositions have temperature independent average coordination numbers of ~ 6, consistent with the liquid structure resembling the high-pressure β-tin structure. A shoulder is apparent on the high-Q side of the first peak in all of the measured $S(Q)$ functions. Atomistic models generated from RMC simulations constrained to the measured $S(Q)$ data indicate that this shoulder may be related to the presence of atomic clusters characterized by interatomic distances shorter than covalent bonds in crystal structures. The shoulder becomes well defined on supercooling, which supports, albeit indirectly, the existence of a transition towards a metastable low-density liquid (LDL) state comprised of tetrahedral clusters with covalent bonding consistent with the ambient-pressure crystal structure.

The use of element selective analysis techniques, such as NDIS or EXAFS, would be invaluable to obtain detailed measurements of the partial structure factors and pair distribution functions of the liquid alloys, in order to gain more detailed insight into the structural evolution upon supercooling. Indeed, the structure of liquid Si$_{20}$Ge$_{80}$ was measured recently by NDIS [57]. The results of these studies will provide powerful additional constraints for molecular simulations to provide a detailed description of the structural mechanisms of the LDL-HDL transformation observed in these metallic melts during deep supercooling.

Acknowledgements

References

[1] Hansen M 1958 *Constitution of Binary Alloys*, (McGraw-Hill)

[2] Harame D L and Meyerson B S, 2001 *IEEE Transactions on Electron Devices* **48** 2555-2567

[3] Rücker H and Heinemann B 2018 *Semicond. Sci. Technol.* **33** 114003

[4] Cressler J D and Niu G F, 2003 *Silicon-Germanium Heterojunction Bipolar Transistors*, (Artech House)

[5] Capper P 2017 *Bulk crystal growth. In: Springer handbook of electronic and photonic materials* (Kasap S and Capper P Eds)

[6] Glazov V M, and Shchelikov O D 2000, *High. Temp.* **38** 405

[7] Glazov V M, Chizhevskaya S N, and Glagoleva N N *1969 Liquid Semiconductors* (New York: Plenum)

[8] Bundy F P 1964 *J. Chem. Phys* **41** 3809

[9] Waseda Y 1980 *Structure of Non-Crystalline Materials* (New York: McGraw-Hill)

[10] Salmon P S, 1988 *J . Phys. F: Met. Phys.* **18** 2345

[11] Waseda Y, Shinoda K, Sugiyama K, Takeda S, Terashima K, Toguri J M 1995 *Jpn. J. Appl. Phys.* **34** 4124

[12] Takeda S 1995, *Jpn. J. Appl. Phys.* **34** 4889

[13] Ansell S, Krishnan S, Felten J J and Price D L 1998 *J. Phys. Cond. Matter* **10** L73

[14] Naito Y, Inui M, Anai T and Tamura K 2007 *J. Non-Cryst. Solids* **353** 3376

[15] Krishnan S, Hennet L, Key T, Glorieux B, Saboungi M-L, Price D L 2007 *J. Non-Cryst. Solids* **353** 2975

[16] Hines A L, Walls H A, Kanhaiyalal R J 1985 *Metal. Trans. A* **16** 267

[17] Schenk T, Holland-Moritz D, Simonet V, Bellissent R and Herlach D M 2002 *Phys. Rev. Lett.* **89** 075507

[18] Rapoport E 1967 *J. Chem Phys.* **46** 2891

[19] McMillan P F, Wilson M, Wilding M C, Daisenberger D, Mezouar M, and Greaves G N 2007 *J. Phys. Condens. Matter* **19** 415101

[20] Filipponi A and Di Cicco A 1995 *Phys. Rev. B* **51**, 12322

[21] McMillan P F, Greaves G N, Wilson M, Wilding M C, Daisenberger D 2013 *Liquid Polymorphism, Book Series: Advances in Chemical Physics* **152** 309

[22] Sastry S and Angell C A 2003 *Nat. Mater.* **2** 739

[23] Kim T H, Lee G W, Sieve B, Gangopadhyay A K, Hyers R W, Rathz T J, Rogers J R, Robinson D S, Kelton K F and Goldman A I 2005 *Phys. Rev. Lett.* **95** 085501

[24] Inui M, Matsusaka T, Ishikawa D, Sakaguchi Y, Hong X, Kazi M H and Tamura K 2001 *J. Synchr. Rad.* **8** 767

[25] Ko E, Jain M and Chelikowsky J R 2002 *J. Chem. Phys.* **117** 3476

[26] Wang Q, Chang J and Wang H P 2019 *Mater. Chem. Phys.* **221** 224-231

[27] Hennet L, Thiaudière D, Gailhanou M, Landron C, Coutures J-P and Price D L 2002 *Rev. Sci. Instrum.* **73** 124

[28] Labiche J-C, Mathon O, Pascarelli S, Newton A A, Guilera Ferre G, Curfs C, Vaughan G, Homs A, Fernandez Carreiras D 2007 *Rev. Scient. Instrum.* **78** 091301

[29] Hammersley A P, Svensson S O, Hanfland M, Fitch A N and Häusermann D 1996 *High Pressure Research* **14** 235-248

[30] Hennet L, Cristiglio V, Kozaily J, Pozdnyakova I, Fischer H E, Bytchkov A, Drewitt J W E, Leydier M, Thiaudière D, Gruner S, Brassamin S, Zanghi D, Cuello G J, Koza M, Magazù S, Greaves G N and Price D L 2011 *Eur. Phys. J. Special Topics* **196** 151–165

[31] Drewitt J W E, Jahn S and Hennet L 2019 *J. Stat. Mech.: Theory Exp.* **10** 104012

[32] Krishnan S, Hansen G, Hauge R and Margrave 1990 *J High Temp. Sci.* **29** 17

[33] Olesinski, R W and Abbaschian, G J 1984 *Bull. of Alloy Phase Diag.* **5** 180–183

[34] Yamasue E, Susa M, Fukuyama H and Nagata K 2002 *J. Cryst. Growth* **234** 121–131

[35] Drewitt J W E, Jahn S, Cristiglio V, Bytchkov A, Leydier M, Brassamin S, Fischer H E and Hennet L. 2011 *J. Phys. Condens. Matter* **23** 155101

[36] Rim W-K and Ohsaka K 2000 *J. Cryst. Growth* **208** 313

[37] "Modeling and Precise Experiments of Diffusion Phenomena in Melts under Microgravity" Annual Reports 2002, NASDA-TMR-030005E

[38] McGreevy R L 2001 *J. Phys.: Cond. Matter* **13** R877

[39] Finney L 1977 *Nature* **266** 309

[40] Medvedev N N 1986 *J. Comput. Phys.* **67** 223

[41] Price D L, Moss S C, Reijers R, Saboungi M-L and Susman S 1998 *J. Phys. C: Sol. State Phys.* **21** L1069

[42] Moss S C and Price D L, physics of Disordered Materials, ed. D. Adler, H Fritzsche and S R Ovchinsky (New York, Plenum, 1985)

[43] Drewitt J W E, Turci F, Heinen B J, Macleod S G, Qin F, Kleppe A K and Lord O T 2020 *Phys. Rev. Lett.* **124** 145501

[44] Roik A S, Kazimirov V P and Sokolskii V E 2004 *J. Struct. Chem.* **45** 648

[45] Stich I, Car R and Parrinello M 1989 *Phys. Rev. Lett.* **63** 2240

[46] Stich I, Car R and Parrinello M 1991 *Phys. Rev. B* **44** 4262

[47] Ogawa H and Waseda Y 1994 *Z. Naturforsch* **49a** 987

[48] Petkov V, Takeda S, Waseda Y and Sugiyama K 1994 *J. Non-Cryst. Solids* **168** 97

[49] Rodriguez S E and Pings C J 1965 *J. Chem. Phys.* **42** 2435

[50] Waseda Y and Suzuki K 1971 *Phys. Stat. Solidi* **47** 581

[51] Isherwood S P and Orton B R 1968 *Phil. Mag.* **17** 561

[52] Narushima T, Hattori T, Kinoshita T, Hinzmann A and Tsuji K, 2007 *Phys. Rev. B* **76** 104204

[53] Tsai K H, Wu T M, Tsay S F and Yang T J 2007 *J. Phys.: Cond. Matter* **19** 205141

[54] Jank W and Hafner J. 1990 *Phys. Rev. B* **41** 1497

[55] Morishita T 2006 *Phys. Rev. Lett.* **97** 165502

[56] Hugouvieux V, Farhi E, Johnson M R, Juranyi F, Bourges P and Kob W 2007 *Phys. Rev. B* **75** 104208

[57] Weis H., Holland-Moritz D., Kargl F. ,Unruh T., Hansen T., Bednarcik J. and Meyer A. to be Submitted

[58] Chai J-D, Stroud D, Hafner J and Kresse G 2003 *Phys. Rev. B* **67** 104205

[59] Beye M, Sorgenfrei F, Schlotter W F, Wurth W and A Föhlisch 2010 *PNAS* **107** 16772